ITS INSTITUTE
Intelligent Transportation Systems

Dual Frequency, Carrier Phase Differential GPS Augmentation

Final Report

Prepared by:

Eddie Arpin
Bryan Newstrom
Craig Shankwitz

Department of Mechanical Engineering
Intelligent Vehicles Laboratory
University of Minnesota

CTS 11-09

Technical Report Documentation Page

1. Report No. CTS 11-09	2.	3. Recipients Accession No.	
4. Title and Subtitle Dual Frequency, Carrier Phase Differential GPS Augmentation		5. Report Date May 2011	
		6.	
7. Author(s) Eddie Arpin, Bryan Newstrom, Craig Shankwitz		8. Performing Organization Report No.	
9. Performing Organization Name and Address Intelligent Vehicles Lab University of Minnesota Department of Mechanical Engineering 111 Church St. SE Minneapolis, MN 55455		10. Project/Task/Work Unit No. CTS Project #2007093	
		11. Contract (C) or Grant (G) No.	
12. Sponsoring Organization Name and Address Hennepin County, 300 6th St S, Minneapolis, MN 55415 Minnesota Valley Transit Authority, 100 E. Highway 13, Burnsville, MN 55337 ITS Institute, University of Minnesota, 511 Washington Ave SE Minneapolis, MN 55455		13. Type of Report and Period Covered Final Report	
		14. Sponsoring Agency Code	
15. Supplementary Notes http://www.its.umn.edu/Publications/ResearchReports/			

16. Abstract (Limit: 250 words)

For many roadway applications, high-accuracy in-lane level vehicle position information is desired. Unfortunately, in many roadway environments GPS dead zones hinder sufficient GPS position accuracy. These roadway environments include underpasses, tree canopies, urban canyons, and any other locations where the view to the sky is limited.

This report introduces a high-accuracy position estimator that augments GPS in areas where short-term (< 200 meter and < 15 second) GPS dead zones exist. The position estimator fuses differential GPS (DGPS) position measurements, yaw rate measurements, and two-dimensional velocity measurements to provide in-lane level accuracy position estimates. The estimator increases the availability of high-accuracy position estimates for applications that demand continuous high-accuracy in-lane level positioning, such as lane departure warning systems.

The position estimator was evaluated and the position accuracy was quantified. Seven vehicles were outfitted with the position estimator system. Data was collected for 460 DGPS outages and the accuracy of the system was analyzed. From the analysis the position accuracy of the estimator could be approximated based on the distance and time since the DGPS outage began. This analysis provides a level of confidence in the position estimates as a function of distance and time elapsed from the start of a DGPS outage. This level of confidence measure allows applications to have a means to reject position estimates based on the outage time and distance if those estimates are projected to have lower accuracy than the application requires.

17. Document Analysis/Descriptors Differential Global Positioning System, Dual frequency, Radio frequency, Carrier phase, Radar receivers, Virtual reference station, Augmentation system, Kinematics		18. Availability Statement No restrictions. Document available from: National Technical Information Services, Springfield, Virginia 22161	
19. Security Class (this report) Unclassified	20. Security Class (this page) Unclassified	21. No. of Pages 43	22. Price

Dual Frequency, Carrier Phase Differential GPS Augmentation

Final Report

Prepared by:

Eddie Arpin
Bryan Newstrom
Craig Shankwitz

Department of Mechanical Engineering
Intelligent Vehicles Laboratory
University of Minnesota

May 2011

Acknowledgments

Table of Contents

List of Figures

List of Tables

Executive Summary

For many roadway applications, high-accuracy in-lane level vehicle position information is desired. Unfortunately, in many roadway environments GPS dead zones hinder sufficient GPS position accuracy. Environments such as these include underpasses, tree canopies, urban canyons, and any other locations where the view to the sky is limited. Periods of degraded GPS solutions, i.e., solution qualities inferior to fixed integer carrier phase solutions, can last from a few seconds to minutes. This report details a real-time estimator used to calculate high-accuracy (centimeter level) estimates of global vehicle position by fusing dual carrier phase differential GPS (DGPS) measurements, high-accuracy vehicle heading measurements, yaw rate measurements, and two-dimensional velocity sensor measurements. This real-time high-accuracy position estimator is needed to augment GPS in environments where spatially periodic GPS dead zones exist. The estimator increases the availability of high-accuracy position estimates for applications that demand continuous high-accuracy, in-lane level positioning, such as lane departure warning systems.

The estimator can be described in three separate parts: the heuristic filter, heading estimator, and the position propagator. Every time a GPS measurement becomes available (GPS measurements are provided at 10 Hz), the heuristic filter updates the position estimate and determines the measurement error covariance of the vehicle heading measurement used in the heading estimator. The heading estimator determines vehicle heading at 10 Hz by using successive GPS measurements, two dimensional velocity measurements, and yaw rate estimates to measure the vehicle heading. A "look-back" approach is used to correct for heading errors. A Kalman filter is used to provide optimal estimates of the vehicle heading and yaw rate bias from input measures of vehicle heading and yaw rate.

The position estimator was evaluated on Minnesota State Highway 77 for use in a lane departure warning system. Ten 40-foot Gillig transit buses were outfitted with the DGPS augmentation system, and position data was collected for 460 bridge induced DGPS outages using seven of the ten buses. These DGPS outages occur when the bridge impairs the GPS receiver's view of the GPS satellites and the outage ends when the receiver regains a fixed integer DGPS solution. When correction signals are available to the GPS receiver, acquiring a fixed integer DGPS solution takes approximately six to ten seconds once GPS satellites are visible. A vehicle traveling 30 miles per hour (13.4 m/s) will travel approximately 90 to 170 meters during a bridge induced DGPS outage (for a six and ten second outage, respectively), depending on the width of the bridge and the reacquisition time.

Seven buses were chosen for the evaluation of the position estimator to identify any performance sensitivity from vehicle to vehicle. Although care was taken to install sensor suites and computational equipment as consistently as possible across each vehicle, different hardware and small differences in sensor locations and orientations create the possibility of performance variance between vehicles.

The primary application for the DGPS augmentation position estimator at this time is for lane departure warning systems for transit buses operating on authorized highway road shoulders. These highway road shoulders have radius of curvatures of greater than 580 meters, which magnifies the importance of lateral accuracy over longitudinal accuracy when the primary

concern is for accurate lateral placement of the vehicle within the shoulder lane. Therefore, lateral position error was chosen as the metric to quantify the performance of the position estimator. Lateral position error is measured by comparing position estimates by the augmentation system to fixed integer DGPS position measurements provided by the Trimble R7 GPS receiver. These real-time kinematic (RTK) DGPS measurements are provided with error-correction information from a Trimble Virtual Reference System (VRS), which provides position accuracy on the order of a few centimeters. Table 2 (recreated below) summarizes the aggregate data of the bridge induced DGPS outages from all seven vehicles.

Table 2. Summary of aggregate data results.

	Lateral Error (m)	Speed (mph)	Speed (m/s)	Outage Time (s)	Outage Distance (m)	Samples
Mean	$8.9832 *10^{-3}$	29.4226	13.1531	9.5952	126.8676	460
Standard Deviation	0.1716	3.3948	1.5176	2.5560	38.9337	--

The data statistics show a mean of 0.898 cm, which supports that the position estimator is unbiased. The position estimates have a lateral error standard deviation of 17.16 cm, and if a normal distribution is assumed, approximately 95.5% of the position estimates are within plus or minus 34.3 cm of the measured value.

The data in Table 3 (recreated below) show that the mean lateral error for each vehicle is within 3.6 cm of the aggregate mean of 0.898 cm. The standard deviations are all within 25 percent of the aggregate standard deviation of 0.1716 m. From this data it is reasonable to conclude, that from the present amount of data collected, the performances of the vehicles are consistent with one another.

Table 3. Lateral error statistics for each vehicle evaluated.

Bus Number	Mean Lateral Error (m)	Lateral Error Standard Deviation (m)	Samples
4577	0.0258	0.1863	62
4580	-0.0214	0.1818	62
4581	0.0167	0.1701	67
4730	-0.0287	0.1384	69
4731	0.0450	0.2146	67
4733	-0.0120	0.1570	68
4734	0.0315	0.1622	65

The data were also broken down for each bridge that caused the DGPS outage, and then aggregated for all seven vehicles, shown in Table 4 (recreated below).

Table 4. Lateral error statistics of DGPS outages per bridge.

Bus Number	Mean Lateral Error (m)	Lateral Error Standard Deviation (m)	Samples
Cliff Northbound	0.0770	0.1490	82
Cliff Southbound	0.0546	0.1339	77
Diffley Northbound	-0.0031	0.1748	82
Diffley Southbound	0.0034	0.1430	71
Hwy 13 Northbound	0.0124	0.1867	77
Hwy 13 Southbound	-0.0891	0.1891	71

The standard deviations of each data set are all within 22 percent of the aggregate standard deviation of 0.1716 m. These standard deviations seem fairly consistent across all of the bridges inside the testing environment, but the mean of the lateral errors seem to vary. Highway 13 southbound and Cliff Road northbound differ from the aggregate mean by 9.81 cm and 6.80 cm respectively. Why the mean error at these locations varies from the mean is unexplained at this time.

Using these lateral error measurements, a first order relationship between distance travelled during a GPS outage and lateral error bounds was developed. This model predicts lateral error as a function of distance travelled, and can be used to reject position estimates when *a priori* acceptable error bounds are exceeded.

Future work, using higher grade yaw rate sensors, is planned. This future work will help analyze the error sources in the position estimates from the estimator, i.e., yaw rate bias estimate errors and random walk errors in the yaw rate sensor. The future work will also provide higher position accuracies due to higher accuracy yaw rate measurements.

1 Introduction

For many roadway applications, high-accuracy in-lane level vehicle position information is desired. Unfortunately, in many roadway environments GPS dead zones hinder sufficient GPS position accuracy. Environments such as these include underpasses, tree canopies, urban canyons, and any other locations where the view to the sky is limited. Degraded GPS solutions, i.e., solution qualities inferior to fixed integer carrier phase solutions, can last from a few seconds to minutes. This report details a real-time estimator used to calculate a high-accuracy (centimeter level) estimates of global vehicle position by fusing dual carrier phase differential GPS (DGPS), high-accuracy vehicle heading measurements, yaw rate measurements, and two-dimensional velocity sensor measurements. This real-time high-accuracy position estimator is needed to augment GPS in environments where spatially periodic GPS dead zones exist.

The goal of this work is to provide high-accuracy position estimates to a lane departure warning system for transit buses operating on authorized road shoulders while the GPS position measurement accuracy is degraded, i.e. solution quality inferior to fixed integer carrier phase solution [1]. The following equipment was used to ensure that the estimator meets the specified centimeter level accuracy:

- A Trimble Zephyr dual carrier phase GPS antenna is mounted on the front of the vehicle with a Trimble R7 GNSS Receiver
- A Crossbow IMU440 inertial measurement unit is mounted securely to the vehicle, and provides vehicle yaw rate measurements
- A Correvit S-350 Aqua two dimensional velocity sensor measures the two dimensional (x, y) velocity vector in the Correvit's (velocity sensor's) local coordinate frame.

The sensor locations are shown in Figure 1.1 below. Detailed sensor specifications can be found in the Appendix.
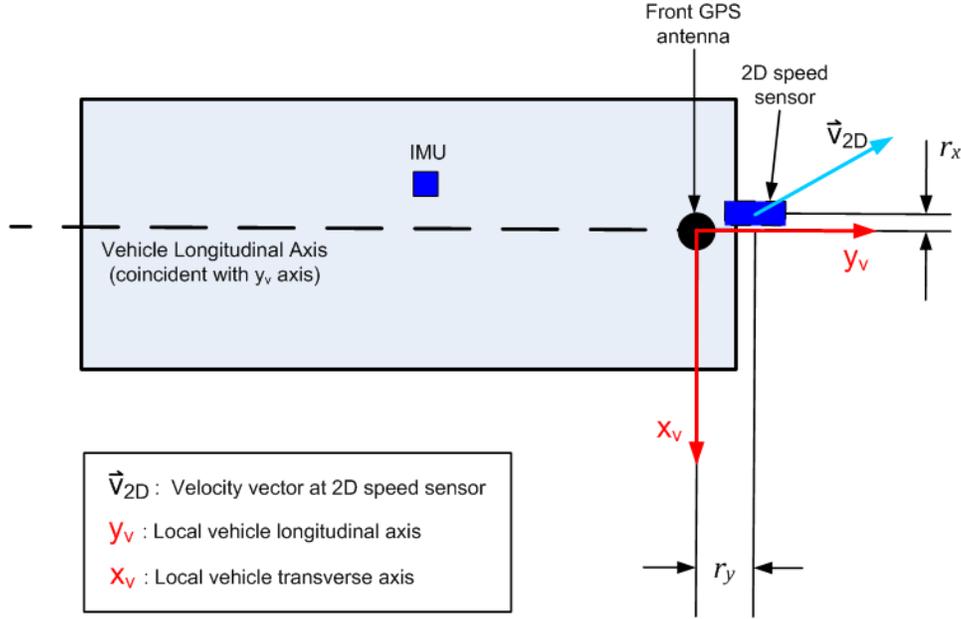
Figure 1.1. Vehicle sensor locations.

1.1 Nomenclature

The general convention used in this report is to cap a measurement variable with a tilde (~) and an estimated value with a hat (^). If the value is not capped it denotes the true value. For example, X_G is the global Easting position in state plane coordinates, so $\tilde{X}_G$ is the measured value provided by GPS and $\hat{X}_G$ is the estimated value of global Easting from the estimator. The following will be the variable notation used throughout this report (refer to Figure 1.2 below).

1.1.1 Coordinate Frames
    1.1.1.1 XSP YSP: State plane coordinate system
    1.1.1.2 $x_v\,y_v$: Local vehicle coordinate frame (origin is located at front GPS antenna and y_v is parallel to the longitudinal axis of the vehicle)
    1.1.1.3 X' Y': State plane coordinate system translated to a point of interest
1.1.2 States
    1.1.2.1 $X_{G,k}$: Global Easting of the vehicle with respect to the state plane coordinate system at time step k
    1.1.2.2 $Y_{G,k}$: Global Northing of the vehicle with respect to the state plane coordinate system at time step k
    1.1.2.3 Ψ_k: Vehicle heading as seen in Figure (angle between y_v axis and East, positive direction is counter-clockwise) at time step k
   1.1.2.4 $\dot{\Psi}_{b,k}$: Yaw rate bias at time step k
1.1.3 Measurements
    1.1.3.1 $\tilde{\Psi}_k$: Vehicle heading measurement at time step k
    1.1.3.2 $\dot{\tilde{\Psi}}_k$: Yaw rate measurement from yaw rate sensor at time step k
    1.1.3.3 $\tilde{\dot{x}}_k$: Velocity parallel to the local vehicle xv-axis at time step k

2

1.1.3.4 $\tilde{y}_k$: Velocity parallel to the local vehicle y_v-axis at time step k

1.1.3.5 $\tilde{X}_{G,k}$: GPS measurement of global Easting from the front GPS unit (state plane coordinates) at time step k

1.1.3.6 $\tilde{Y}_{G,k}$: GPS measurement of global Northing from the front GPS unit (state plane coordinates) at time step k
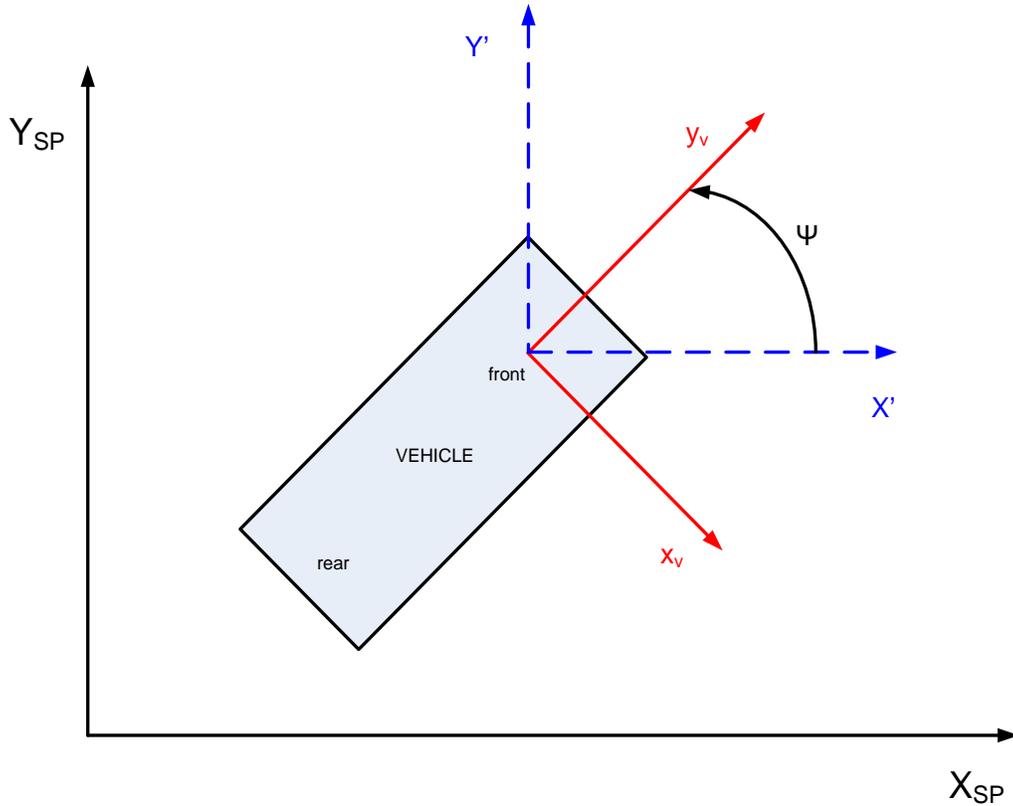

Figure 1.2. Vehicle coordinate system and vehicle heading depiction.

1.2 *Vehicle Position and Heading Estimator Overview*

The estimator can be split into three separate parts: the heuristic filter, heading estimator, and the position propagator. Every time a GPS measurement becomes available (GPS measurements are provided at 10 Hz) the heuristic filter updates the position estimate and determines the measurement error covariance (R values) of $\tilde{\Psi}_k$ for the heading estimator. The heading estimator measures vehicle heading at 10 Hz by using successive GPS measurements, two dimensional velocity measurements and yaw rate estimates to measure the vehicle heading in the past and then to propagate it to the present, which will be referred to as the "look-back" method. A Kalman filter is used to provide optimal estimates of the vehicle heading and yaw rate bias from input measures of vehicle heading and yaw rate. The estimated vehicle heading is propagated from IMU information at 100 Hz.

The position propagator uses kinematic equations to integrate-out position estimates using data from the two dimensional velocity sensor and yaw rate sensor at 100 Hz. The entire process is depicted in the data flowchart shown in Figure 1.3.

3
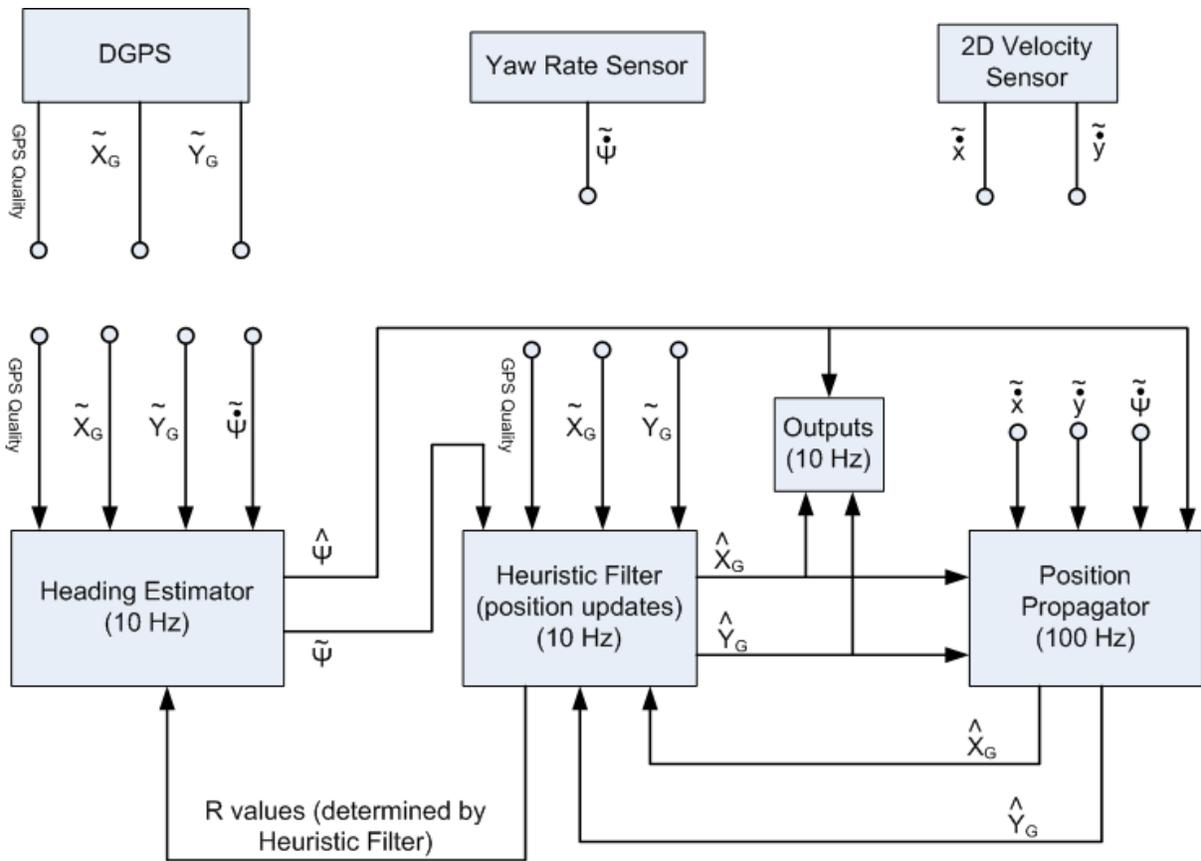
Figure 1.3. Estimator flowchart.

2   Method

2.1   Position Propagator

The position state equations are used to propagate the state estimates of $X_{G,k}$ and $Y_{G,k}$ between GPS measurements. The other states, Ψ_k and $\dot{\Psi}_{b,k}$, will be updated by the heading estimator. The state matrix for the position propagator is defined as

Equation 1

$$x_{P,k} = \begin{bmatrix} X_{G,k} \\ Y_{G,k} \end{bmatrix}$$

The following is the derivation of the state equations for the system of the form

Equation 2

$$\hat{x}_{P,k+1} = \hat{x}_{P,k} + \Delta t \cdot \hat{\dot{x}}_{P,k}$$

Equation 3

$$\hat{\dot{x}}_{P,k} = \begin{bmatrix} \hat{\dot{X}}_{G,k} \\ \hat{\dot{Y}}_{G,k} \end{bmatrix}.$$

Here, $\hat{x}_{P,k+1}$ is the state matrix estimate at time step k+1, Δt is the difference in time between time steps k and k+1, and $\hat{\dot{x}}_P$ is the rate of the change of the estimated state matrix at time step k.

The two-dimensional velocity sensor measures the velocity vector at time step k:

Equation 4

$$\tilde{\vec{V}}_{2D,k} = \begin{bmatrix} \tilde{\dot{x}}_k \\ \tilde{\dot{y}}_k \\ 0 \end{bmatrix},$$

at the location of the velocity sensor. Note that the velocity in the z dimension is not measured by the two-dimensional velocity sensor; thus it is shown as zero. Translating the velocity at the velocity sensor, $\tilde{\vec{V}}_{2D,k}$, to the velocity at the origin of the local vehicle coordinate frame at time step k, $\tilde{\vec{V}}_{v,k}$,

Equation 5

$$\vec{\tilde{V}}_{v,k} = \vec{\tilde{V}}_{2D,k} - \vec{\omega}_k \times \vec{R} = \begin{bmatrix} \tilde{x}_k + r_y \widehat{\dot{\Psi}}_k \\ \tilde{y}_k - r_x \widehat{\dot{\Psi}}_k \\ 0 \end{bmatrix}$$

where $\vec{R} = \begin{bmatrix} r_x \\ r_y \\ 0 \end{bmatrix}$ (r_x and r_y are shown in Figure 1.1), $\vec{\omega}_k = \begin{bmatrix} 0 \\ 0 \\ \widehat{\dot{\Psi}}_k \end{bmatrix}$ and $\widehat{\dot{\Psi}}_k = \widetilde{\dot{\Psi}}_k - \widehat{\dot{\Psi}}_{b,k}$,

the estimate of the vehicle's yaw rate at time step k.

To transform the local vehicle velocity, $\vec{V}_{v,k}$, to the global state plane velocity, we must pre-multiply $\vec{V}_{v,k}$ by the rotation matrix

$$\begin{bmatrix} \sin(\Psi_k) & \cos(\Psi_k) & 0 \\ -\cos(\Psi_k) & \sin(\Psi_k) & 0 \\ 0 & 0 & 0 \end{bmatrix}.$$

Thus,

Equation 6

$$\widehat{\dot{X}}_G = \left(\tilde{x}_k + r_y \widehat{\dot{\Psi}}_k \right) \sin(\Psi_k) + \left(\tilde{y}_k - r_x \widehat{\dot{\Psi}}_k \right) \cos(\Psi_k), \text{ and}$$

Equation 7

$$\widehat{\dot{Y}}_G = - \left(\tilde{x}_k + r_y \widehat{\dot{\Psi}}_k \right) \cos(\Psi_k) + \left(\tilde{y}_k - r_x \widehat{\dot{\Psi}}_k \right) \sin(\Psi_k).$$

Putting the state equations into discrete matrix form, then

Equation 8

$$\hat{x}_{P,k+1} = \begin{bmatrix} \hat{X}_{G,k+1} \\ \hat{Y}_{G,k+1} \end{bmatrix} = \begin{bmatrix} \hat{X}_{G,k} \\ \hat{Y}_{G,k} \end{bmatrix} + \Delta t \begin{bmatrix} \left(\tilde{x}_k + r_y \widehat{\dot{\Psi}}_k \right) \sin(\Psi_k) + \left(\tilde{y}_k - r_x \widehat{\dot{\Psi}}_k \right) \cos(\Psi_k) \\ -\left(\tilde{x}_k + r_y \widehat{\dot{\Psi}}_k \right) \cos(\Psi_k) + \left(\tilde{y}_k - r_x \widehat{\dot{\Psi}}_k \right) \sin(\Psi_k) \end{bmatrix}.$$

2.2 Heading Estimator

The heading estimator measures the vehicle heading from a look-back algorithm, and uses the vehicle heading and yaw rate measurements in a linear Kalman filter to estimate the yaw rate bias and vehicle heading. The look-back algorithm uses the previous GPS position, two-dimensional velocity measurements and yaw rate estimates to measure vehicle heading. Because of the relatively long baseline distance between the first and last GPS measurement in the succession of measurements, an accurate measurement of vehicle heading can be calculated.

Even at vehicle speeds of 2.23 meters per second the baseline length between the first and last GPS measurement would be approximately 6.7 meters assuming a straight line path and a three second "look-back window."

2.2.1 Look-back Algorithm

Step One:

The position estimate at time t_{n-m} is propagated to the most recent time step occurring at time t_n. This is accomplished by using Equation 9 and Equation 10 with the position and vehicle heading estimates at time t_{n-m} as the initial conditions along with m values of time, two dimensional velocity measurements and yaw rate estimates from time t_{n-m} to t_n.

Equation 9

$$\begin{bmatrix} \hat{X}_{G,t_n} \\ \hat{Y}_{G,t_n} \end{bmatrix} = \begin{bmatrix} \hat{X}_{G,t_{n-m}} \\ \hat{Y}_{G,t_{n-m}} \end{bmatrix} + \sum_{i=n-m}^{n-1} (t_{i+1} - t_i) \begin{bmatrix} \left(\tilde{x}_i + r_y \hat{\dot{\Psi}}_i \right) \sin \alpha + \left(\tilde{y}_i - r_x \hat{\dot{\Psi}}_i \right) \cos \alpha \\ -\left(\tilde{x}_i + r_y \hat{\dot{\Psi}}_i \right) \cos \alpha + \left(\tilde{y}_i - r_x \hat{\dot{\Psi}}_i \right) \sin \alpha \end{bmatrix}$$

Equation 10

$$\alpha = \hat{\Psi}_{t_{n-m}} + \sum_{p=n-m}^{i} (t_{p+1} - t_p) \hat{\dot{\Psi}}_p$$

Figure 2.1 illustrates this position propagation from the initial conditions at time t_{n-m} to the last occurring time step at time t_n.
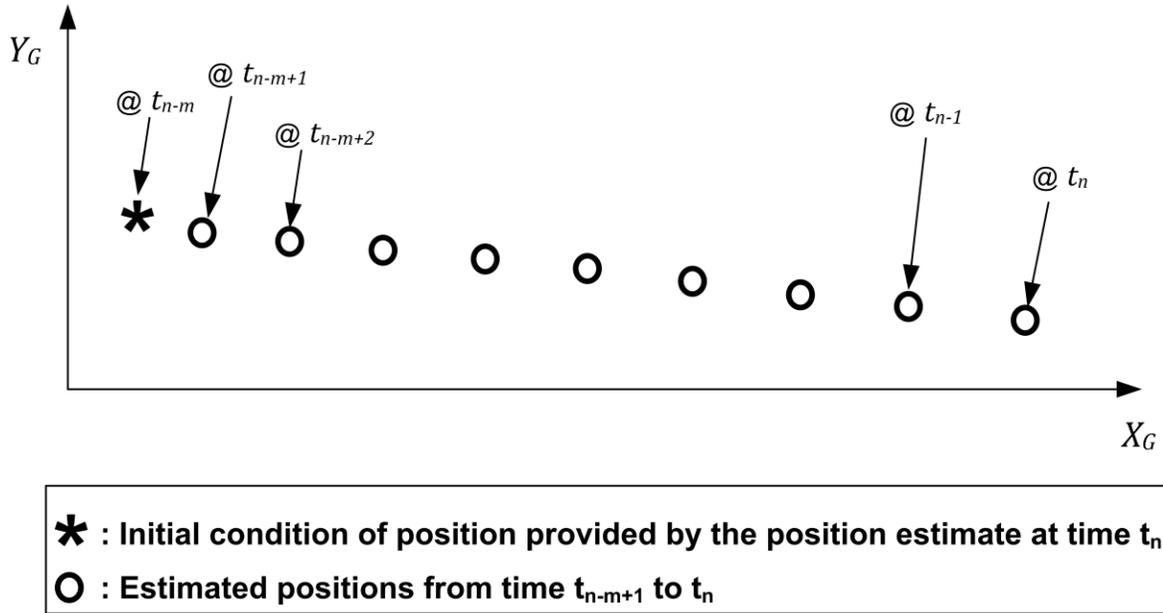
Figure 2.1. Position propagation from time t_{n-m} to t_n.

Step Two:

The projected position trajectory from step one is then compared to the measured GPS position trajectory. The lateral position error between the two position trajectories is used to compensate for the errors associated with the initial vehicle heading estimate. It is assumed that the majority of the lateral position error between the GPS measured trajectory and the position estimates is due to the error in the initial vehicle heading used to propagate the position in step one. Figure 2.2 shows a depiction of GPS position measurements overlaid onto the position propagation estimates from step one.
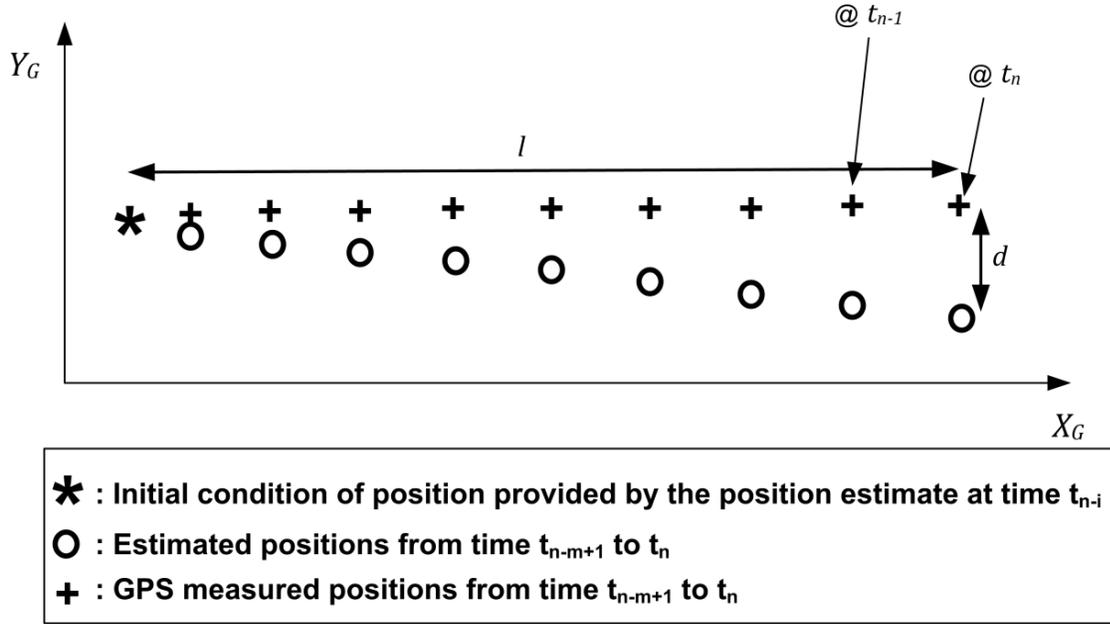
Figure 2.2. Comparison of GPS and estimated position trajectory.

The lateral position error between the GPS trajectory and the estimated positions is defined as

Equation 11

$$d = \frac{\begin{bmatrix} \hat{X}_{G,t_n} - \hat{X}_{G,t_{n-1}} \\ \hat{Y}_{G,t_n} - \hat{Y}_{G,t_{n-1}} \end{bmatrix} \times \begin{bmatrix} \tilde{X}_{G,t_n} - \tilde{X}_{G,t_{n-1}} \\ \tilde{Y}_{G,t_n} - \tilde{Y}_{G,t_{n-1}} \end{bmatrix}}{\begin{vmatrix} \hat{X}_{G,t_n} - \hat{X}_{G,t_{n-1}} \\ \hat{Y}_{G,t_n} - \hat{Y}_{G,t_{n-1}} \end{vmatrix}}.$$

The path length of the measured GPS trajectory, l, is defined as

Equation 12

$$l = \sum_{i=n-m}^{n-1} \begin{vmatrix} \tilde{X}_{G,t_i} - \tilde{X}_{G,t_{i+1}} \\ \tilde{Y}_{G,t_i} - \tilde{Y}_{G,t_{i+1}} \end{vmatrix}.$$

The angle between the estimated position trajectory and the measured GPS position trajectory is then computed

Equation 13

$$\theta = tan^{-1} \frac{l}{d}$$

Step Three:

The angle between the estimated position trajectory and the measured GPS position trajectory, θ, computed in step two, is then used to compute an "optimal" vehicle heading measurement at time step t_{n-m}. If this "optimal" vehicle heading measurement were used as the initial condition to propagate the position estimates using Equation 9 and Equation 10 again, as in step one, the propagated position estimates would overlay directly over the GPS measured position trajectory and the lateral error between the two trajectories would be zero. This "optimal" vehicle heading measurement is then propagated from time step t_{n-m} to the current time step t_n using the yaw rate estimates from the m time steps.

Thus,

Equation 14

$$\tilde{\Psi}_{t_n} = \tilde{\Psi}_{t_{n-m}} + \sum_{i=n-m}^{n-1}(t_{i+1} - t_i)\hat{\dot{\Psi}}_i,$$

where the yaw rate estimates are defined as

Equation 15

$$\hat{\dot{\Psi}}_i = \tilde{\dot{\Psi}}_i - \hat{\dot{\Psi}}_{b,i}.$$

At each time step t_n, these three steps are repeated, thereby providing a continuous stream of accurate vehicle heading measurements. This process is computationally inexpensive, and straightforward to implement.

2.3 Linear Kalman Filter

The Kalman filter is responsible for producing optimal estimates of the vehicle heading, $\hat{\Psi}_k$, and the yaw rate bias, $\hat{\dot{\Psi}}_{b,k}$, in the presence of sensor measurement noise. The state matrix of the linear Kalman filter is

Equation 16

$$x_{KF,k} = \begin{bmatrix} \Psi_k \\ \dot{\Psi}_{b,k} \end{bmatrix}.$$

The generic discrete-time linear Kalman filter system model is of the form

Equation 17

$$x_{KF,k+1} = \Phi_k x_{KF,k} + \Gamma u_k + Y w_k, \quad w_k \sim N(0, Q_k),$$

Equation 18

$$\tilde{y}_k = H x_{KF,k} + v_k, \quad v_k \sim N(0, R_k),$$

where w_k and v_k are the input noise and measurement noise respectively; w_k and v_k are modeled by zero-mean Gaussian distributions. The input noise error covariance, Q_k, is related to the error characteristics of the yaw rotation rate measurement from the Crossbow IMU unit. The observation noise, R_k, is related to the quality of the heading measurement, and is determined by the heuristic filter explained in the following section. The specific system model for the linear Kalman filter is below:

Equation 19

$$\begin{bmatrix} \Psi_{k+1} \\ \dot{\Psi}_{b,k+1} \end{bmatrix} = \begin{bmatrix} 1 & -\Delta t \\ 0 & 1 \end{bmatrix} \begin{bmatrix} \Psi_k \\ \dot{\Psi}_{b,k} \end{bmatrix} + \begin{bmatrix} \Delta t \\ 0 \end{bmatrix} \tilde{\dot{\Psi}} + \begin{bmatrix} -\Delta t \\ 0 \end{bmatrix} w_k$$

Equation 20

$$\tilde{y}_k = \tilde{\Psi}_k = \begin{bmatrix} 1 & 0 \end{bmatrix} \begin{bmatrix} \Psi_k \\ \dot{\Psi}_{b,k} \end{bmatrix} + v_k.$$

The state estimate $\hat{x}_{KF}$, and the state error covariance, P, are both propagated when a new yaw rate measurement is available (100 Hz) and a measurement update is performed when a new heading measurement is available (10 Hz). A summary of the state and state error covariance propagation, gain computation, and measurement update is shown in Table 1 [2].

Table 1. Summary of linear Kalman Filter steps.

Gain Computation	**Equation 21** $$K_k = P_k H^T [H P_k H^T + R_k]^{-1}$$
Measurement Update	**Equation 22** $$\hat{x}_{KF,k+1} = \hat{x}_{KF,k} + K_k\big[\tilde{y}_k - H\hat{x}_{KF,k}\big]$$ **Equation 23** $$P_{k+1} = [I - K_k H]P_k$$
Propagation	**Equation 24** $$\hat{x}_{KF,k+1} = \Phi_k \hat{x}_{KF,k} + \Gamma u_k$$ **Equation 25** $$P_{k+1} = \Phi_k P_k \Phi^T + Y Q_k Y^T$$

2.4 Heuristic Filter

The "Heuristic Filter" block, shown in Figure 1.3, determines the position update gain value, $K_{PG,k}$, and vehicle heading observation error covariance (R_k values) for the position update equation and linear Kalman filter, respectively. When the position update gain value is determined, the heuristic filter uses the incoming GPS position measurements, $\begin{bmatrix}\tilde{X}_{G,k}\\\tilde{Y}_{G,k}\end{bmatrix}$, to update the position estimates, $\begin{bmatrix}\hat{X}_{G,k}\\\hat{Y}_{G,k}\end{bmatrix}$, by using the following equation:

Equation 26

$$\begin{bmatrix}\hat{X}_{G,k+1}\\\hat{Y}_{G,k+1}\end{bmatrix} = \begin{bmatrix}\hat{X}_{G,k}\\\hat{Y}_{G,k}\end{bmatrix} + K_{PG,k}\left[\begin{bmatrix}\tilde{X}_{G,k}\\\tilde{Y}_{G,k}\end{bmatrix} - \begin{bmatrix}\hat{X}_{G,k}\\\hat{Y}_{G,k}\end{bmatrix}\right].$$

The position update gain and vehicle heading error covariance are selected based on the following metrics:

- *GPS quality* – Ranges between fix, float, DGPS, autonomous, and no solution. These values provide GPS solution quality information. A fix solution implies that the integer ambiguities in the carrier phase measurement have been solved with a certain level of confidence.

- d_k – The distance between the DGPS measurement and the estimator's position estimate, $\left\| \begin{bmatrix} \tilde{X}_{G,k} \\ \tilde{Y}_{G,k} \end{bmatrix} - \begin{bmatrix} \hat{X}_{G,k} \\ \hat{Y}_{G,k} \end{bmatrix} \right\|$

- $\dfrac{\Delta \tilde{\Psi}_k}{\Delta t_k}$ – The computed heading measurement derivative with respect to time, i.e.,

Equation 27

$$\frac{\Delta \tilde{\Psi}_k}{\Delta t_k} = \frac{\tilde{\Psi}_k - \tilde{\Psi}_{k-1}}{t_k - t_{k-1}}.$$

The basic logic of how these metrics were used to select the position update gain and heading measurement observation error covariance is shown below in Figure 2.3.
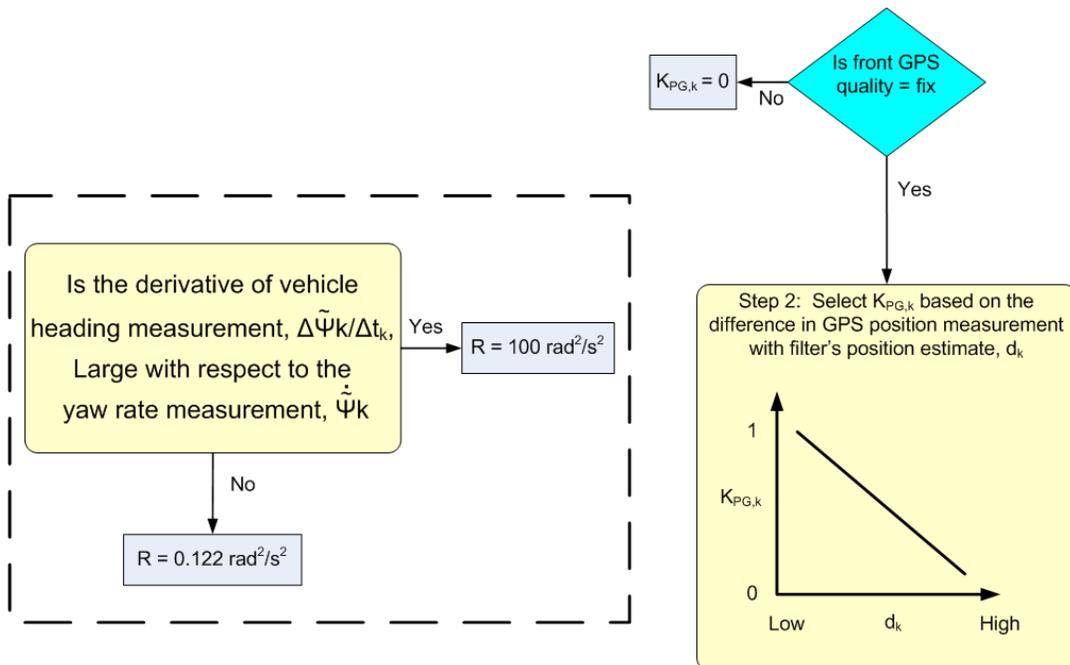
Figure 2.3. Heuristic filter logic.

3   Results

Ten 40-foot Gillig transit buses were outfitted with the DGPS augmentation system, and seven of these buses were used to collect data for 460 bridge induced DGPS outages. These DGPS outages occur when the bridge impairs the GPS receiver's view of the GPS satellites and the outage ends when the receiver regains a fixed integer DGPS solution. When correction signals are available to the Trimble R7 GPS receiver, acquiring a fixed integer DGPS solution takes approximately six to ten seconds once GPS satellites are visible. A vehicle traveling 30 miles per hour (13.4 m/s) will travel approximately 90 to 170 meters during a bridge induced DGPS outage, depending on the width of the bridge and the reacquisition time.

3.1   Vehicles

Seven buses were chosen for the evaluation of the position estimator to identify any performance sensitivity from vehicle to vehicle. Although care was taken to install sensor suites and computational equipment as consistently as possible across each vehicle, different hardware and small differences in sensor locations and orientations create the possibility of performance variance between vehicles. The 40-foot Gillig Phantom bus model used in the evaluation is shown below in Figure 3.1.

Figure 3.1. 40 foot Gillig Phantom (Bus 2.0).

3.2 Data Collection

The testing environment was Minnesota State Highway 77, south of Old Shakopee Road and north of Interstate 35-E, as shown in Figure 3.2. Seven vehicles were driven underneath Cliff Road, Diffley Road, and Minnesota State Highway 13 underpasses to provide DGPS outages while traveling on Highway 77. For the entirety of the data collection, the vehicles traveled on bus authorized road shoulders on Highway 77. These road shoulders stipulate that vehicle speeds be limited to 35 miles per hour or 15.6 meters per second. The data collection includes more than 60 bridge induced DGPS outages per vehicle and 460 total outages for the seven vehicles.
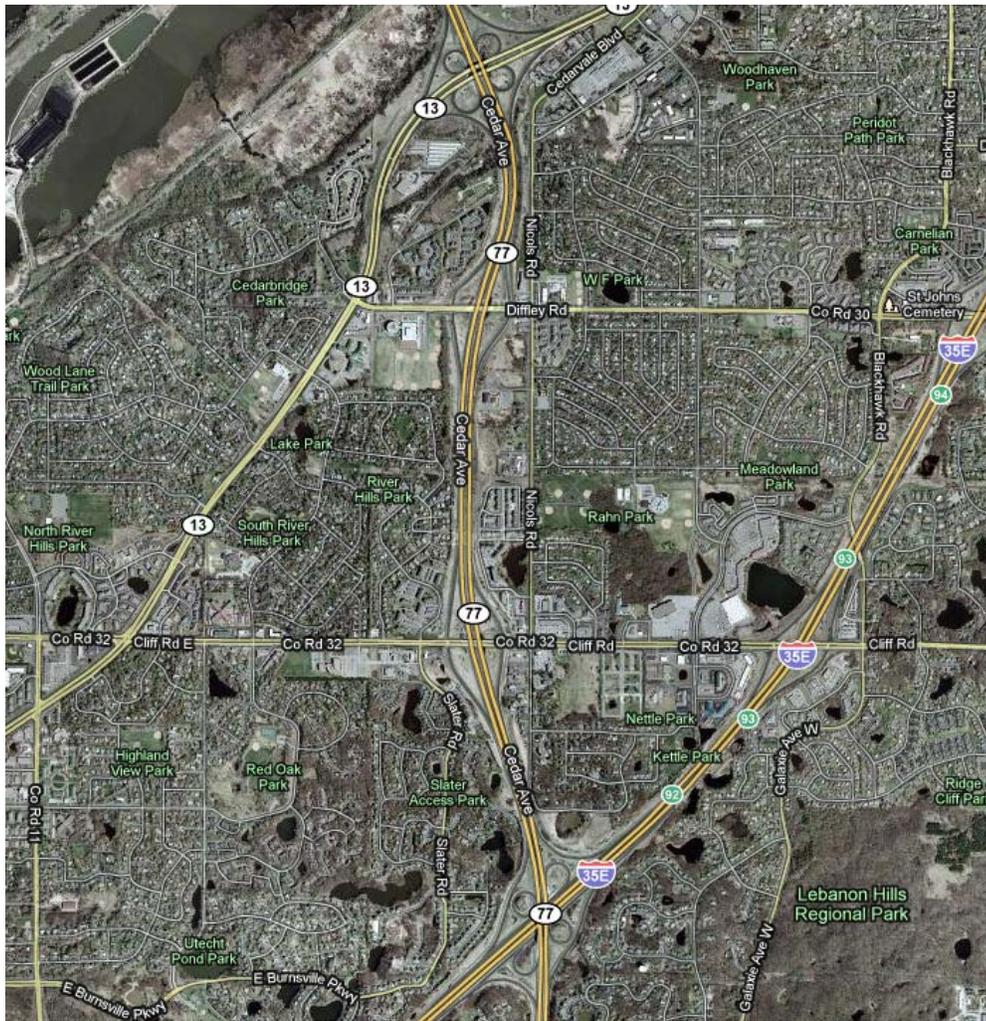

**Figure 3.2. Minnesota State Highway 77.**
©2010 Google Imagery ©2010 TerraMetrics, Map data © Google

3.3 Position Accuracy Metric

The primary application for the DGPS augmentation position estimator at this time is for lane departure warning systems for transit buses operating on authorized highway road shoulders. These highway road shoulders have radius of curvatures of greater than 580 meters [3], which

magnifies the importance of lateral accuracy over longitudinal accuracy when the primary concern is for accurate lateral placement of the vehicle within the shoulder lane. Therefore lateral position error was chosen as the metric to quantify the performance of the position estimator.

Lateral position error is measured by comparing position estimates by the augmentation system to fixed integer DGPS position measurements provided by the Trimble R7 GPS receiver. These real-time kinematic (RTK) DGPS measurements are provided with error-correction information from a Trimble Virtual Reference System (VRS), which provides position accuracy on the order of a few centimeters [4]. A depiction of the lateral error is shown in Figure 3.3 below.

$\ast$ -- GPS position measurement at time step k+1

$\ast$ -- GPS position measurement at time step k

$\bigcirc$ -- Filter position estimate at time step k
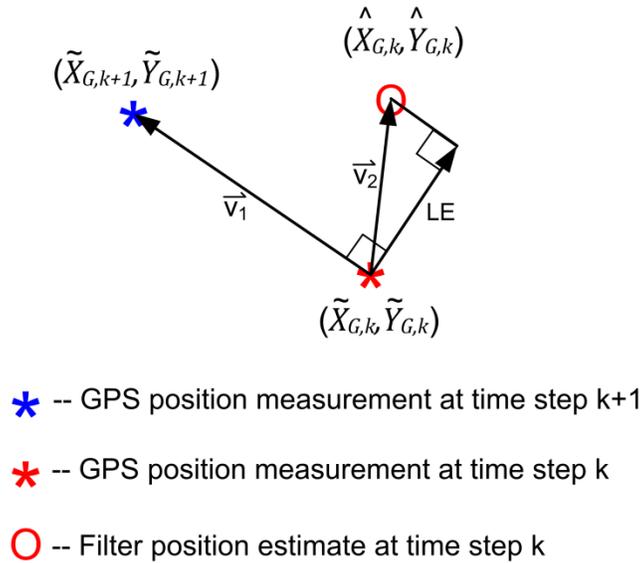
Figure 3.3. Lateral error of DGPS augmentation system.

The lateral error (LE) is computed from the following relationship: $LE = \dfrac{\vec{V}_1 \times \vec{V}_2}{|\vec{V}_1|}$.

3.4   Results

The results in this section quantify the accuracy of the position estimates provided by the estimator. Table 2 summarizes the aggregate data of the bridge induced DGPS outages from all seven vehicles.

Table 2. Summary of aggregate data results.

	Lateral Error (m)	Speed (mph)	Speed (m/s)	Outage Time (s)	Outage Distance (m)	Samples
Mean	$8.9832 * 10^{-3}$	29.4226	13.1531	9.5952	126.8676	460
Standard Deviation	0.1716	3.3948	1.5176	2.5560	38.9337	--

The data statistics show a mean of 0.898 cm, which supports that the position estimator is unbiased. The position estimates have a lateral error standard deviation of 17.16 cm, and if a normal distribution is assumed, approximately 95.5% of the position estimates are within plus or minus 34.3 cm of the measured value.

Figure 3.4 plots the mean and standard error bounds (plus and minus one standard deviation) of the lateral position errors for each of the seven vehicles, and the data that supports this plot is shown in Table 3 below.
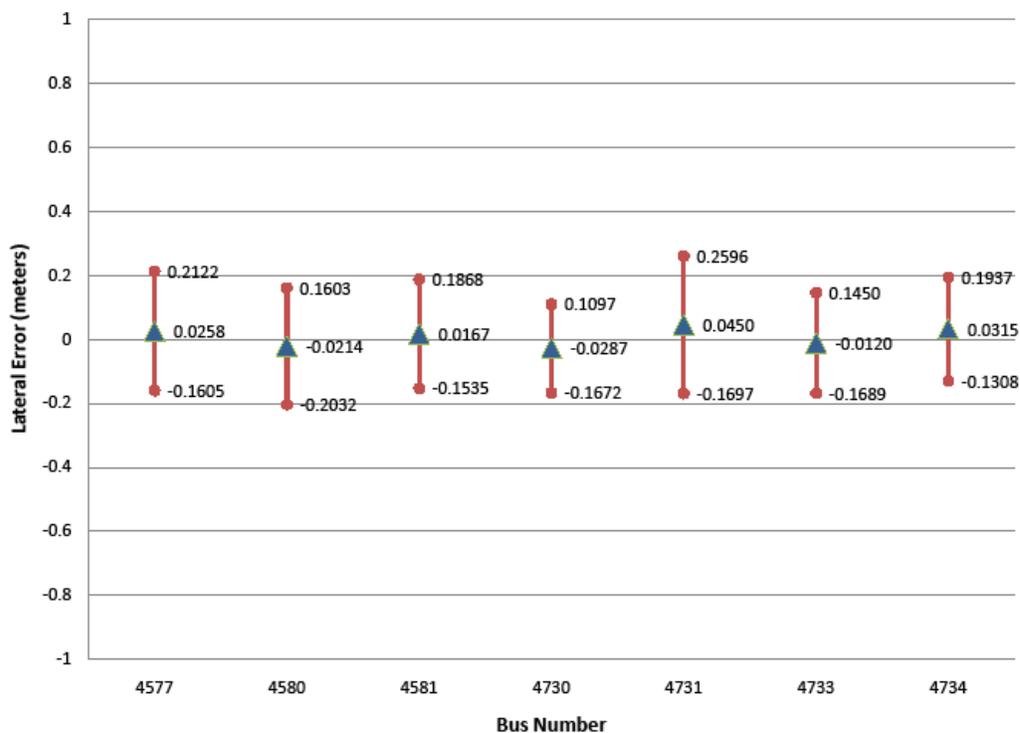

Figure 3.4. Standard error plot of lateral error as a function of vehicle driven.

18

Table 3. Lateral error statistics for each vehicle evaluated.

Bus Number	Mean Lateral Error(m)	Lateral Error Standard Deviation (m)	Samples
4577	0.0258	0.1863	62
4580	-0.0214	0.1818	62
4581	0.0167	0.1701	67
4730	-0.0287	0.1384	69
4731	0.0450	0.2146	67
4733	-0.0120	0.1570	68
4734	0.0315	0.1622	65

The data shows that the mean lateral error for each vehicle is within 3.6 cm of the aggregate mean of 0.898 cm. The standard deviations are all within 25 percent of the aggregate standard deviation of 0.1716 m. From this data it is reasonable to conclude, that from the present amount of data collected, the performances of the vehicles are consistent with one another.

The data was also broken down for each bridge that caused the DGPS outage. This data is an aggregate of all seven vehicles, which is shown in Figure 3.5 below. This data is also summarized in Table 4 below.
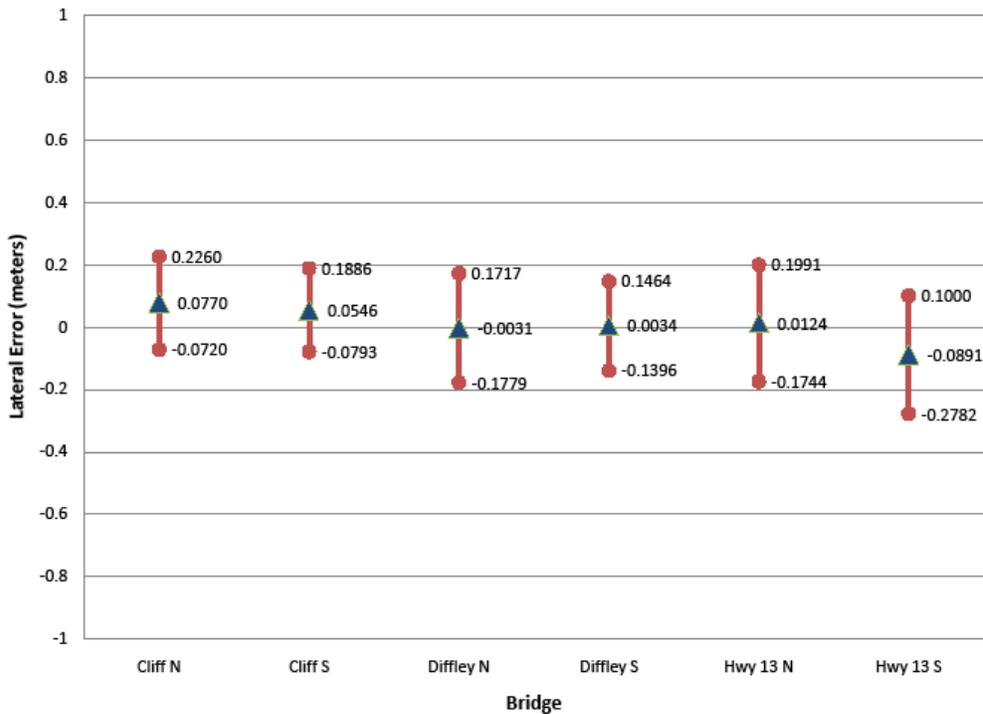
**Figure 3.5. Lateral error as a function of bridge DGPS outage.**

Table 4. Lateral error statistics of DGPS outages per bridge.

Bus Number	Mean Lateral Error (m)	Lateral Error Standard Deviation (m)	Samples
Cliff Northbound	0.0770	0.1490	82
Cliff Southbound	0.0546	0.1339	77
Diffley Northbound	-0.0031	0.1748	82
Diffley Southbound	0.0034	0.1430	71
Hwy 13 Northbound	0.0124	0.1867	77
Hwy 13 Southbound	-0.0891	0.1891	71

The standard deviations of each data set are all within 22 percent of the aggregate standard deviation of 0.1716 m. These standard deviations seem fairly consistent across all of the bridges inside the testing environment, but the mean of the lateral errors seem to vary. Highway 13 southbound and Cliff Road northbound differ from the aggregate mean by 9.81 cm and 6.80 cm respectively. It is inconclusive whether a position estimate bias exists for the augmentation system for these bridges without having significantly more data samples to analyze. Histograms

of lateral error broken down by bridge and vehicle along with the aggregate data set are included in the Appendix.

Lateral error is expected to increase as a function of time and distance from the start of a DGPS outage. Although the initial condition of position is fairly accurate (< 9 cm), any error in the initial heading condition at the start of a DGPS outage will increase the position error linearly as the path distance traveled increases. This effect is shown in Figure 3.6.
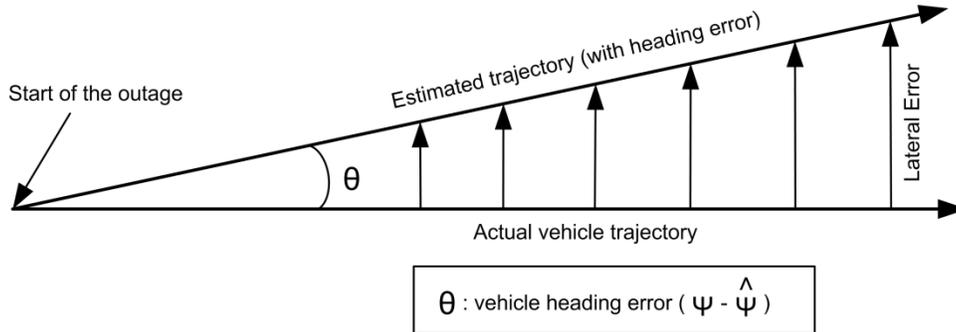
Figure 3.6. Growth in lateral error with the increase in distance traveled due to initial heading error.

If the main source of lateral error is assumed to be caused by the initial heading estimate, the lateral error should increase fairly linearly with distance traveled or time elapsed since the outage began (distance is proportional to time at a constant speed). Therefore a linear model can be used to approximate bounds on lateral error as a function of either distance traveled or elapsed time since the outage began.

The linear relationship between lateral error and distance traveled was determined using all 460 instances of GPS outages recorded. Thus, for each instance, the normalized Lateral Error LE_i is computed to be:

Equation 28

$$NLE_i = \frac{LE_i}{DO_i},$$

where LE_i is the lateral error for outage i, and DO_i is the distance traveled by the vehicle during the outage.

The mean and standard deviation of the set $\{NLE_i\}$ is then used to model the estimated error associated with the augmentation system as a function of either distance traveled or time (assuming constant speed for each instance i). These results are shown in Table 5.

Table 5. Lateral error statistics normalized against distance and time for 460 instances of GPS outages.

	Lateral Error/Distance (m/m)	Lateral Error/Time (m/s)
Mean {NLE_i}	$9.1804 * 10^{-5}$	$9.4511 * 10^{-4}$
Standard Deviation {NLE_i}	$1.3292 * 10^{-3}$	$1.7603 * 10^{-2}$

Figure 3.7 shows the projected lateral error as a function of distance since the start of a DGPS outage. This plot was generated using the results in Table 5. The error bars depict plus and minus one standard deviation.
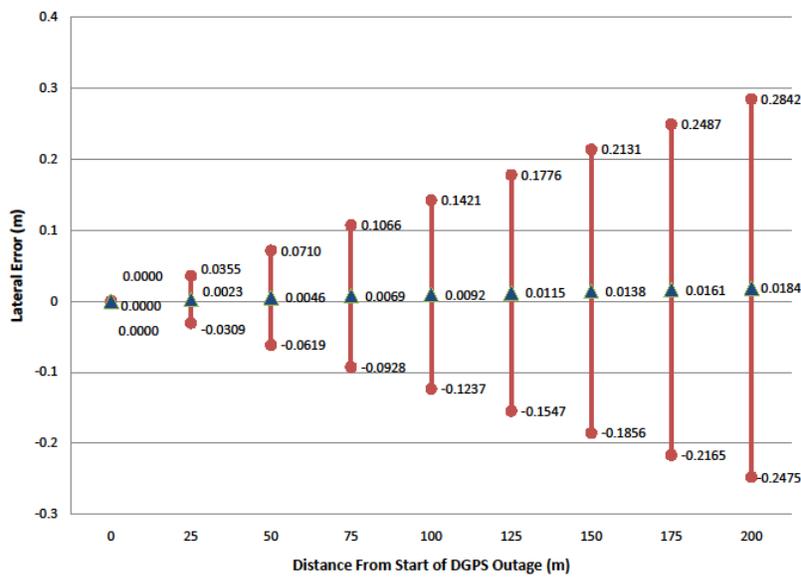
Figure 3.7. Increase in lateral error as a function of distance from start of DGPS outage.

The projected error characteristics in Figure 3.7 were formulated from the results shown in Table 2. It would be expected that if the vehicle speed were lower, the standard deviation of lateral error would increase. This increase in deviation of lateral error would be caused by the increase in amount of time needed to travel the same distance as would be achieved at higher speeds. This increase in time would increase the amount of drift error in the heading estimate, causing the position estimates to increasingly vary from truth.

Under the assumption that lateral error grows linearly with time if vehicle velocity is held constant, Figure 3.8 shows the projected lateral error as a function of time elapsed since the DGPS outage began.
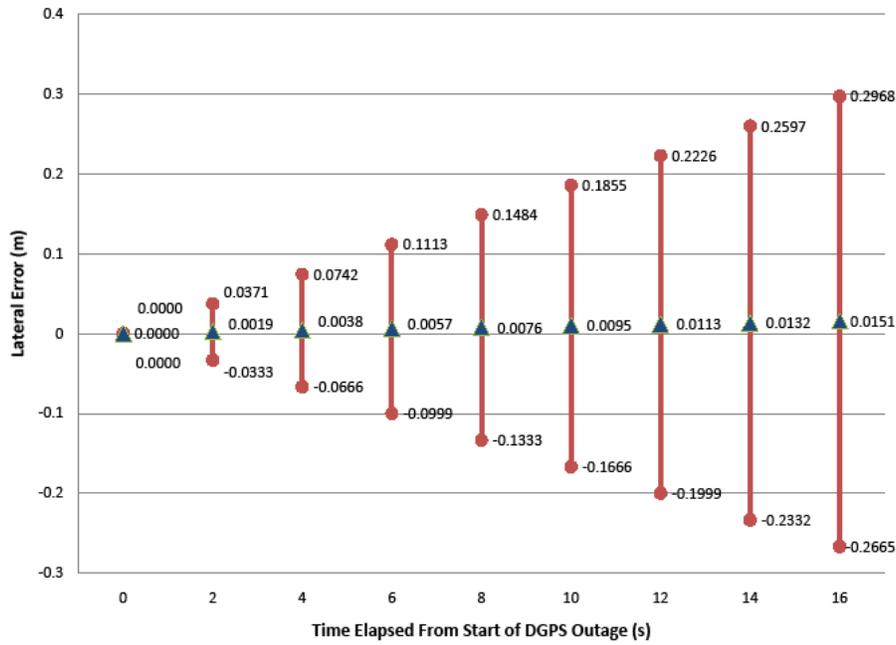
Figure 3.8. Increase in lateral error as a function of outage elapsed time.

As with Figure 3.7, Figure 3.8 is based on the results from Table 5. It would be expected that if the vehicle speeds were lower, the standard deviation of lateral error would decrease. The decrease in distance traveled from the start of the DGPS outage would decrease the lateral error associated with the initial error in the heading estimate, thus decreasing the variance in lateral error as a function of time.

At the time of this report, the assumption is made that the most significant source of position error is the initial heading estimate at the start of the outage. Other potential causes of position error include errors in the yaw rate bias estimate, rapid changes in the yaw rate bias, and bias in the two-dimensional velocity sensor. Future work is planned using a higher accuracy IMU to test this assumption. With a higher accuracy IMU, the effect of the modeling errors in the Crossbow yaw rate sensor can be analyzed.

4   Conclusions

A GPS augmentation position estimator is presented that provides high-accuracy position estimates during DGPS outages. This position estimator is implemented in a lane departure warning system for transit buses traveling on authorized highway shoulders. Ten vehicles were outfitted with the positioning estimator and data was collected using seven of the ten buses on Minnesota State Highway 77. Position data for 460 Bridge induced DGPS outages were collected and analyzed to quantify the positioning accuracy of the position estimator. The aggregate results collected from the seven vehicle installations show a mean lateral position error of 0.898 cm and a standard deviation of 17.16 cm.

The data from seven separate vehicle installations were compared to evaluate any varying performance of the position estimator. The mean lateral position errors were within 3.6 centimeters of the aggregate mean lateral position error of 0.898 cm. The standard deviations were all within 25 percent of the aggregate standard deviation of 0.1716 m. From these statistics, the position estimator showed very low sensitivity to multiple vehicle installations, which includes different vehicles, sensor and computation hardware, and varying sensor locations and orientations.

The data was also separated by each bridge that caused DGPS outages to evaluate any performance sensitivity to the physical environment. Three of the six bridges used in the evaluation had mean lateral position error within 1.5 cm of the aggregate mean, but the other three bridges differed from the aggregate mean by 4.56 cm, 6.80 cm, and 9.81 cm. With the current amount of data collected, whether the augmentation system exhibits a significant bias at these locations is still inconclusive. The standard deviations at each bridge are fairly consistent, as the furthest departure from the aggregate is by 22 percent.

The aggregate data was then normalized against distance and time elapsed since the DGPS outages began. This was done to project the lateral position error characteristics as a function of distance and time from the start of an outage. The plots shown in Figure 3.7 and 3.8 can be used to estimate the drop off in accuracy as time and distance increase from the start of an outage. This analysis can be used to provide various applications, with varying needs of position accuracy, a level of confidence in the position estimates as a function of distance and time elapsed from the start of a DGPS outage. Applications then have a means to reject position estimates based on the outage time and distance if those estimates are projected to have lower accuracy than the application requires.

Future work is planned to analyze the sources of position error by using higher grade GPS and IMU technology. This will give a baseline to compare the sensors used in this report, and lead to a better understanding of the augmentation system's ability to model sensor bias and errors.

References

1. L. Alexander, P. Cheng, M. Donath, A. Gorjestani, B. Newstrom, C. Shankwitz, W. Trach, "DGPS-based Lane Assist System for Transit Buses," *Proceedings of the 2004 Intelligent Transportation Systems Conference*, October 3-6, 2004, pp. 755-760.

2. J. Crassidis, J. Junkins, *Optimal Estimation of Dynamic Systems*, Chapman & Hall/CRC, Boca Raton, FL, 2004.

3. Minnesota Department of Transportation, "Road Design Manual," Design Standards Units, St. Paul, MN, September 2004, pp. 3-2(3a).

4. M. Sergi, B. Newstrom, A. Gorjestani, C. Shankwitz, M. Donath, "Dynamic Evaluation of High-accuracy Differential GPS", *Proceedings of the 2003 National Technical Meeting of the Institute of Navigation*, January 22-24, 2003, pp. 581-592.

Appendix A: DGPS and Augmentation Hardware and Performance Histograms

A.1 Sensor Specifications
A.1.1   Correvit S-350 Aqua Two Dimensional Velocity Sensor

Figure A.1 -- Correvit S-350 Aqua 2D velocity sensor.

Speed Range: 0.5 – 250 Kilometers per hour
Distance Resolution: 2.47 mm
Distance measurement deviation: $<\pm 2\%$

See http://www.corrsys-datron.com/Support/Data_Sheets/Datasheets-Sensors/cds-d_S-350_e.pdf for more detailed specifications

A.1.2   Crossbow IMU440

Figure A.2 -- Crossbow IMU440.

Update rate: 2-100 Hz (programmable)
Angular Rate (^{o}): ± 200
Bias (^{o}/sec): $<\pm 0.75$
Resolution (^{o}/sec): <0.06
Random Walk (^{o}/hr$^{1/2}$): <4.5

See http://www.xbow.com/Products/Product_pdf_files/Inertial_pdf/IMU440_Datasheet.pdf for more detailed specifications

A.1.3   Trimble R7 GPS Receiver and Zephyr Model 2 Antenna


Figure A.3 -- Trimble R7 receiver and Zephyr Model 2 Antenna.

Measurement Frequency: 1-10 Hz. (programmable)
Mean Position Accuracy: < 9.4 cm
Standard Deviation of Position Accuracy: < 8.9 cm

See http://trl.trimble.com/docushare/dsweb/Get/Document-140051/Spec_Sheet_-_R7_-_English.pdf for more detailed specifications

A.2 Lateral Error Histograms
A.2.1 Separated by Vehicle
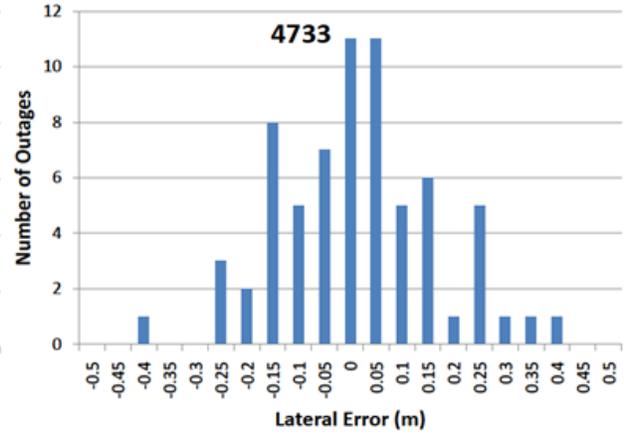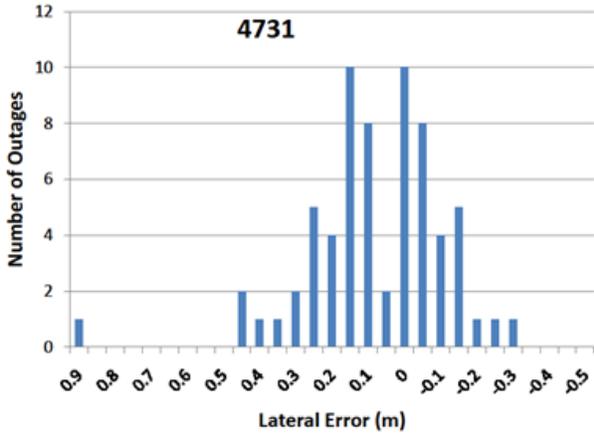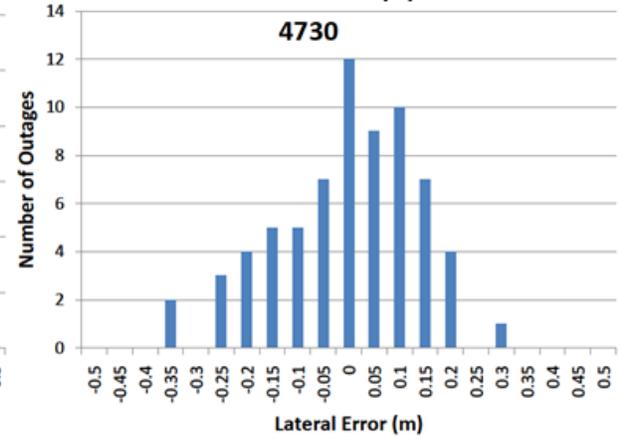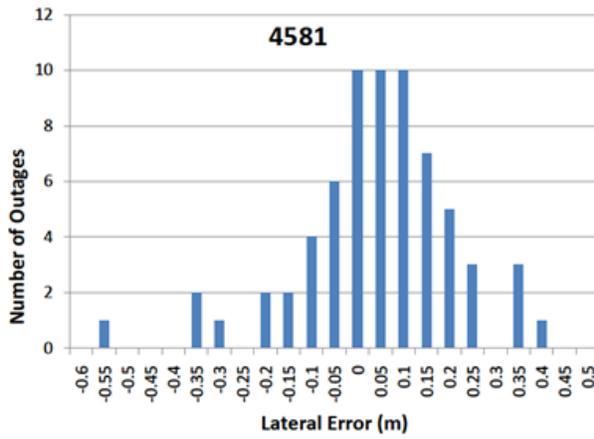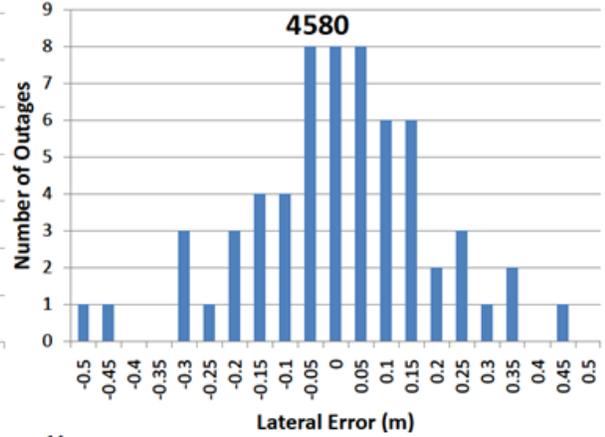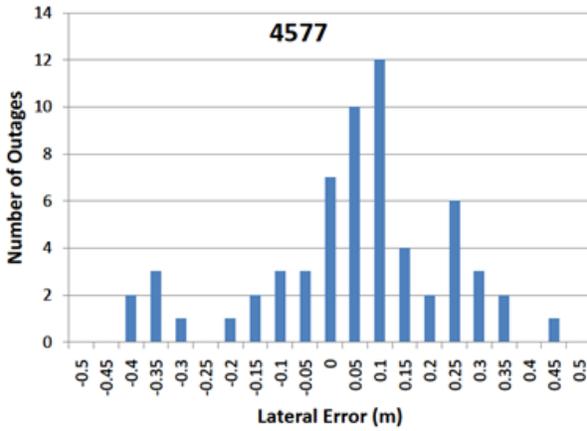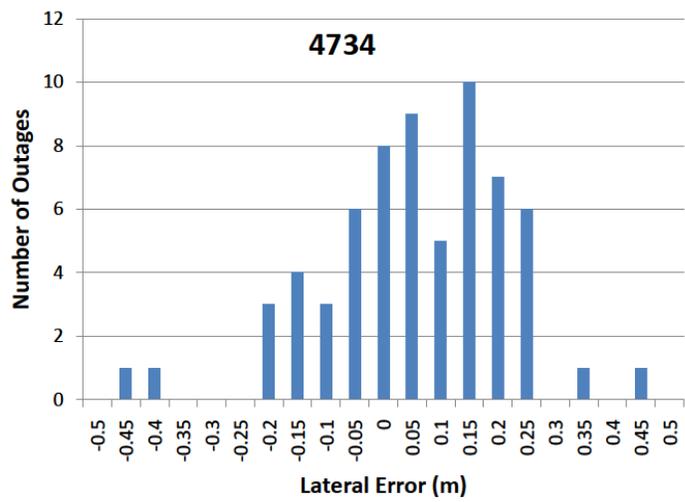
Figure A.4 -- Histograms of lateral error by vehicle.

A.2.2 Separated by Bridge
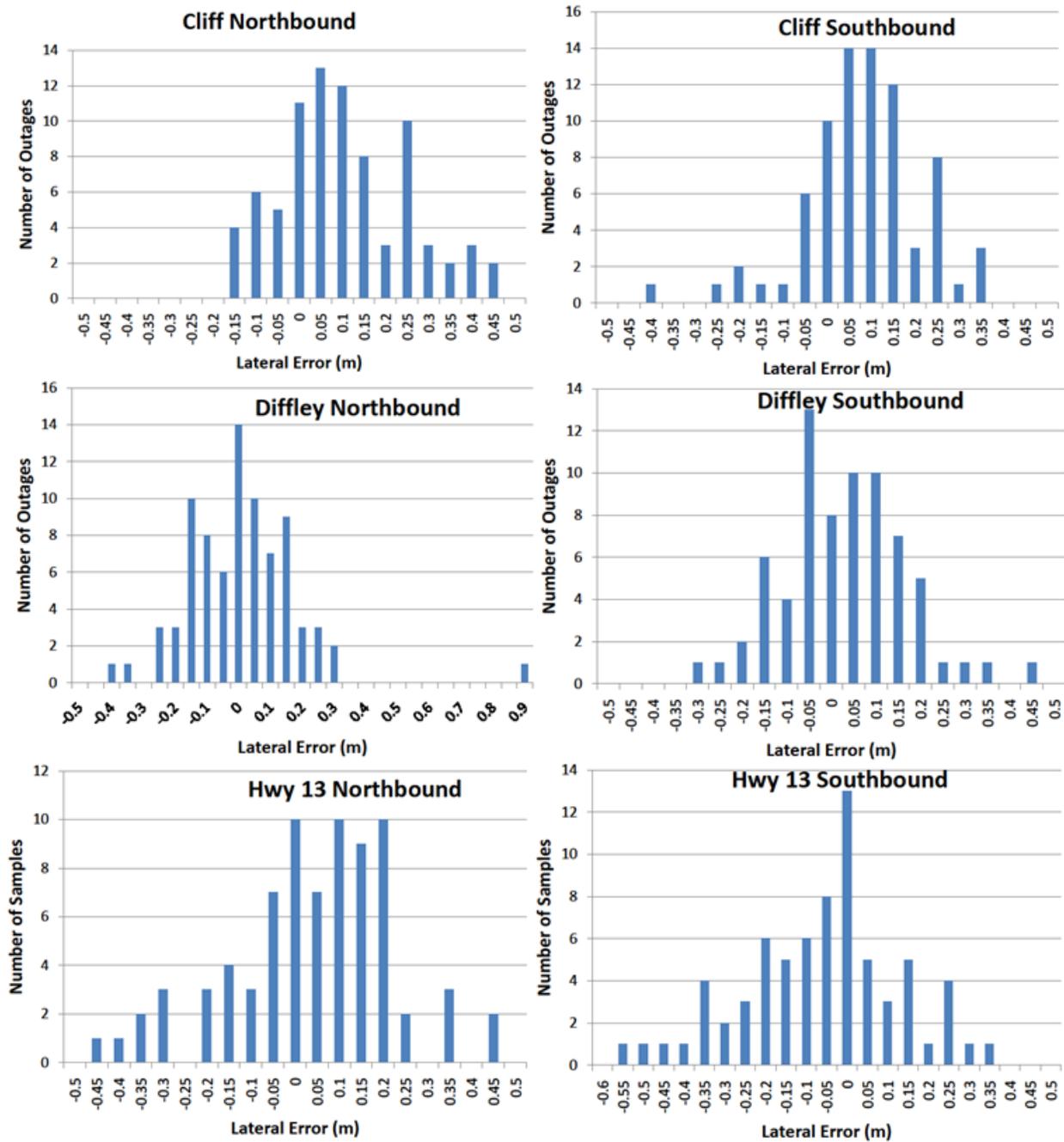
**Figure A.5 -- Histograms of lateral error by bridge.**

A.2.3 Aggregate
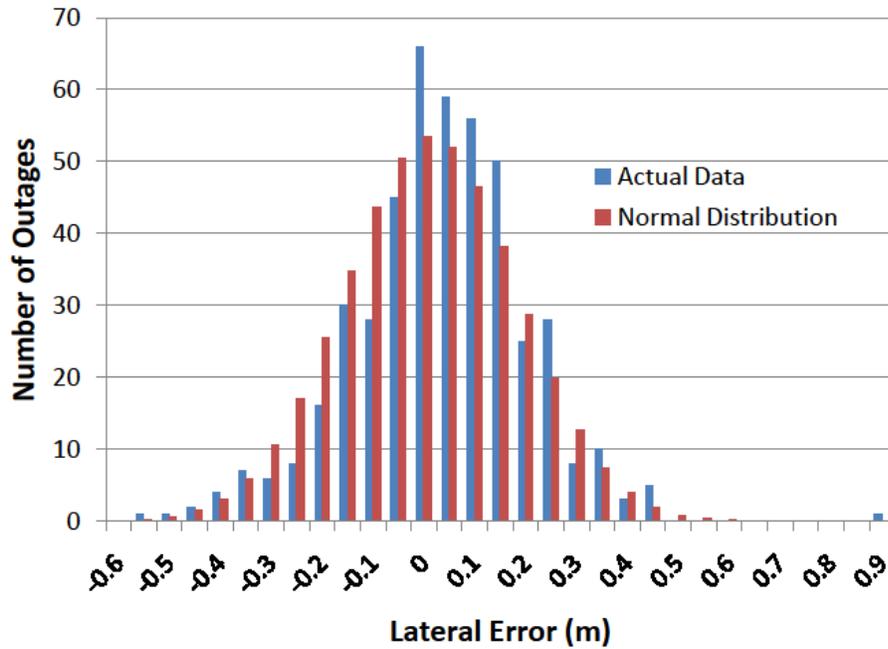
Figure A.6 -- Aggregate histogram of lateral error. Normal distribution fit is also shown to validate the assumption that the actual data is Gaussian.
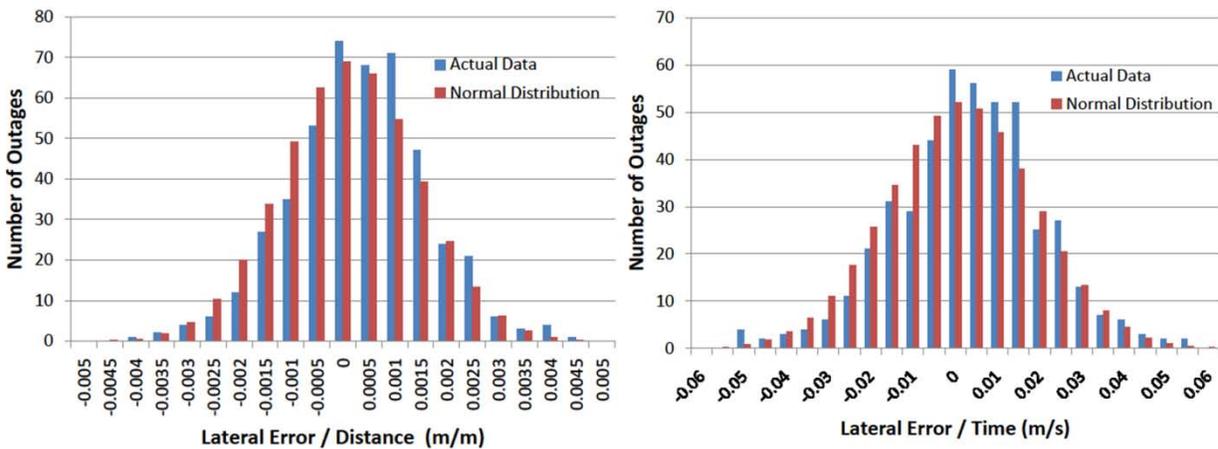

Figure A.7 -- Aggregate histograms normalized by distance and time since start of DGPS outage.